Charge-Density-Shear-Moduli Relationships in Aluminum-Lithium Alloys

Mark Eberhart

Department of Chemistry and Geochemistry, Colorado School of Mines, Golden, Colorado 80401

(Received 13 June 2001; published 26 October 2001)

Using the first principles full-potential linear-augmented-Slater-type orbital technique, the energies and charge densities of aluminum and aluminum-lithium supercells have been computed. The experimentally observed increase in aluminum's shear moduli upon alloying with lithium is argued to be the result of predictable changes to aluminum's total charge density, suggesting that simple rules may allow the alloy designer to predict the effects of dilute substitutional elements on alloy elastic response.

DOI: 10.1103/PhysRevLett.87.205503 PACS numbers: 62.20.Dc, 31.10.+z

Unlike many aspects of mechanical behavior, where the phenomena of interest are controlled by variations of microstructure, elastic response is a consequence of subtle changes to the electron density. Such changes are caused by atomic motions many times smaller than interatomic distances. In turn, these small atomic motions, and the charge redistribution they cause, play a crucial part in mediating plastic deformation. Consequently, a fundamental understanding of the electronic origins of elastic response is crucial to a complete picture of mechanical behavior. In an attempt to develop this picture, researchers are increasingly using the tools of electronic structure theory, which are perfectly tuned to this type of investigation. Previously [1], full-potential linear-augmented-Slater-type orbital (FLASTO) techniques [2,3] were used to investigate the charge redistribution associated with elastic distortion in the elemental fcc metals. Here, this work is extended to alloys, with an investigation of the apparently anomalous increase in the shear moduli of aluminum due to lithium alloying.

Though it has been known since the 1920s that lithium increases aluminum's polycrystalline elastic stiffness [4], intuition suggests otherwise. This expectation is based first on lithium's elastic stiffness, 4.1 GPa, which is enormously lower than that of aluminum, 70.4 GPa. Second, lithium atoms are larger than aluminum atoms, and larger volumes usually correspond to lower elastic stiffness. Third, reasoning thermodynamically, Zener [5] showed that solute atoms of small solubility should lower the tensile modulus when they are dispersed atomically. Despite these contrary expectations, measurements confirm the surprising effect of lithium upon aluminum. These include the work of Noble and co-workers [6], Müller and coworkers [7], and especially Müller [8] who has confirmed the modulus increases and has shown the rate of increase to be a surprising 2% per at.% lithium.

Aluminum-lithium alloys are not only of scientific interest but also of enormous technological importance due to their high stiffness to density ratio, an asset especially to aerospace. Lee and co-workers [9] have given many property-application details, especially with respect to naval aircraft. Lacom [10] has described the technological advantages and disadvantages of aluminum-lithium alloys. In an extensive review, Starke and Staley [11] detail the status of these alloys together with their aerospace applications.

Because of its technological interest and with no experimental methods to detect the shifts of aluminum's charge density with alloying, researchers have turned to first principles methods. These solve the equations of quantum mechanics to find the internal energy and charge density of a molecule or solid. In principle, quantum mechanical calculations can detect the subtlest changes of charge density. In practice, however, there is always the question as to whether the approximations used to make the equations solvable may also obscure the very charge density variations of interest. Though there is no definitive answer to this question, it has been assumed that if the calculated energies recover the phenomenon under investigation, then the underlying cause, hidden in the charge densities, is also recovered. Until quite recently, quantum mechanical methods were not sufficiently accurate to recover the moduli enhancements associated with dilute lithium alloying of aluminum. Müller [8] used Leigh's extension to polyvalent metals of Fuchs's [12] original calculations of elastic constants of alkali metals and copper. Thomas [13,14] applied this method to aluminum's elastic constants and concluded that Leigh's model must be defective, lacking a satisfactory treatment of band-structure effects. Suzuki [15] agreed that Leigh's rigid-band model cannot predict aluminum's elastic constants, and Suzuki carried out Ashcroft local-pseudopotential-model calculations. Despite the clear superiority of Suzuki's calculation over Leigh's model, the predicted C_{ij} were unconvincing. For example, against the observed $C_{44} = 31.6$ GPa, Suzuki predicted a range of 47.1−83.3 GPa. Using a similar pseudopotential, Ledbetter and Suzuki [16] failed to accurately calculate the aluminum-lithium-alloy Young modulus increase, even though they considered third-order perturbation-theory contributions. Benckert [17] also failed to predict aluminum's C_{44} value. However, with improved pseudopotentials and the development of full-potential band-structure techniques, first principles methods are now reliably used to calculate elastic moduli [18]. Eberhart [1] used the FLASTO method to calculate single crystal elastic constants of fcc transition metals.

Iotova and co-workers [19] used methods based on the full-potential linear-muffin-tin orbital approach to study the elastic properties of ordered intermetallic alloys, while Woodward and co-workers [20,21] used pseudopotential approaches to calculate the elastic moduli of aluminum-scandium alloys.

Previous work [1] has uncovered relationships between geometric properties of the charge density and elastic moduli. These structure-property relationships are based on the topological theory due to Bader and co-workers [22–27]. In part, the validity of this theory derives from the homeomorphism between the topology of the charge density, $\rho(r)$, and a molecule's or a solid's network of bonds. With this mapping, a chemical bond is associated with the ridge of maximum charge density connecting two atoms. The existence of such a ridge, and therefore a bond, is guaranteed by the presence of the specific type of critical point. Critical points (cps) occur whenever the gradient of the charge density vanishes, i.e., $\nabla\rho(r) = \vec{0}$. There are necessarily four types of critical points in a three-dimensional space: maxima, minima, and two kinds of saddle points. These may be distinguished by the curvature of $\rho(r)$ in three orthogonal directions, the eigenvalues of the Hessian of the charge density. At a maximum, the curvature is negative in three directions, while at a minimum, it is positive. The first saddle point is characterized by two positive and one negative curvature and the other by one positive and two negative curvatures, necessitating the existence of a ridge of maximum charge density and therefore a bond. For this reason, these critical points are called bond critical points. Bader defined the bond path to be the ridge of maximum charge density connecting two nuclei and passing through the bond cp. Figure 1 shows the total charge density in a [100] plane of aluminum, along with the location of its bond cps and bond paths.

Relationships between geometric properties of the charge density and moduli come through the development of measures allowing bond cps to be compared. By definition, at a bond cp, the Hessian of the charge density has one positive and two negative eigenvalues; hence, there must be directions in which the curvature of the charge density is zero. The locus of all such directions forms an elliptic cone with its apex coincident with the bond cp and its axis parallel to the bond path (Fig. 2). This cone may be parametrized by the two angles ϕ and θ (Fig. 2). The tangents of these angles are related to the relative curvatures of the positive and negative eigenvalues of the Hessian of the charge density.

Letting $\rho_{\parallel\parallel}$ be the curvature of the charge density at the critical point and parallel to the bond path (the positive eigenvalue), while $\rho_{\perp\perp}$ and $\rho_{\perp'\perp'}$ denote the curvatures in the orthogonal perpendicular directions (the negative eigenvalues), then

$$\tan\theta = \left(\frac{\rho_{\perp\perp}}{\rho_{\parallel\parallel}}\right)^{1/2}$$

and

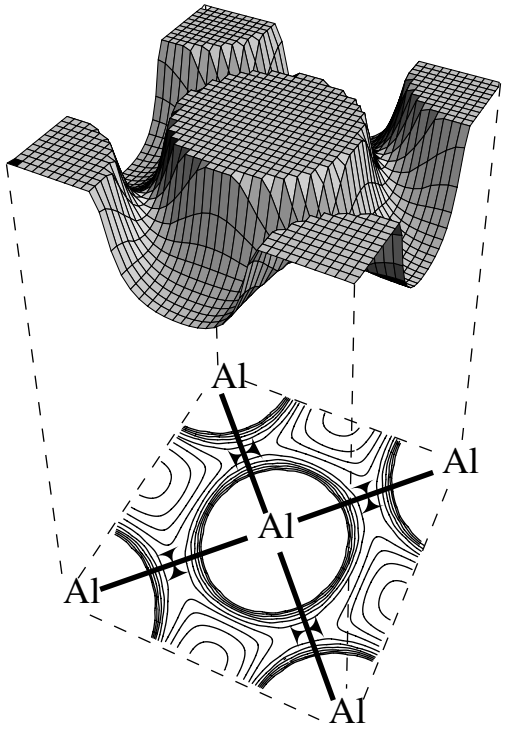

FIG. 1. The charge density in an aluminum (100) plane with bond cps and bond paths shown. The bond paths, shown as lines in the contour plot, represent the ridge of maximum charge density connecting bound atoms. While the magnitude of the charge density may vary from one fcc metal to another, the topology does not and is fully determined by the position and type of critical points.

$$\tan\phi = \left(\frac{\rho_{\perp'\perp'}}{\rho_{\parallel\parallel}}\right)^{1/2}.$$

Relationships between these angles and the single crystal elastic constants of fcc and bcc transition metals have been demonstrated. As an example, Fig. 3 shows the relationship between the C_{44} elastic constants of the fcc metals

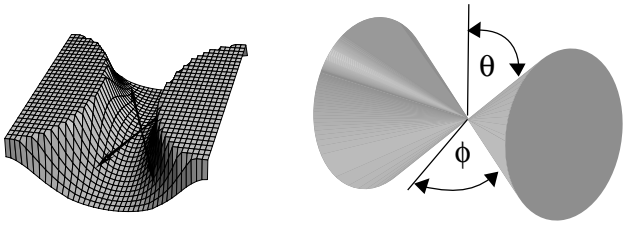

FIG. 2. Left: the directions of zero curvature passing through a bond cp and contained in a (100) plane; right: the locus of all such directions. This locus of directions produces an elliptic cone. The axis of the cone lies along the bond path and coincides with the direction of maximum positive curvature. The magnitude of this curvature is denoted by $\rho_{\parallel\parallel}$ to indicate the second derivative of the charge density parallel to the bond path. The axes of negative curvature are perpendicular to the bond path. The magnitude of these curvatures is denoted as $\rho_{\perp\perp}$ and $\rho_{\perp'\perp'}$. The tangents of the angles θ and ϕ are given by $(\frac{\rho_{\perp\perp}}{\rho_{\parallel\parallel}})^{1/2}$ and $(\frac{\rho_{\perp'\perp'}}{\rho_{\parallel\parallel}})^{1/2}$, respectively.

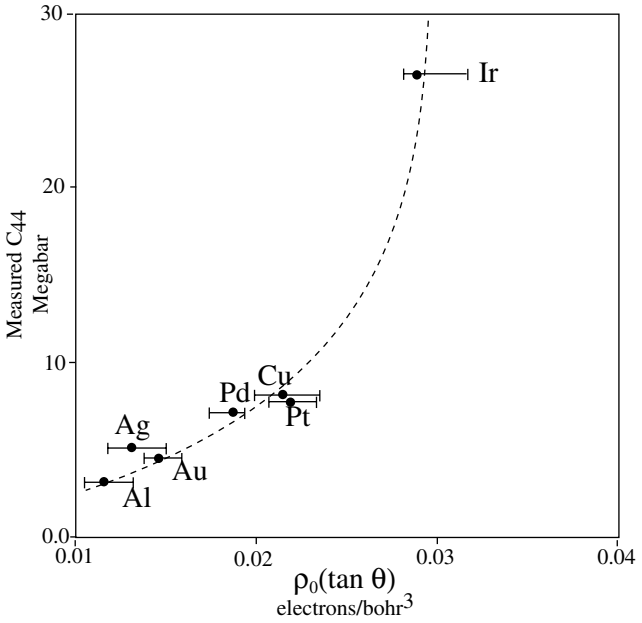

FIG. 3. A plot showing the relationship between the C_{44} elastic constant and $\rho_0 \tan\theta$.

and $\rho_0 \tan\theta$, where ρ_0 is the charge density at the bond cp. With bond directionality frequently evoked as an explanation of single crystal elastic constants, the tangents of the angles between the principal axes of negative curvature and the cone of zero curvature have been defined to be the measure of bond directionality in fcc metals.

Using this definition of bond directionality, the computational strategy to investigate the effects of lithium on the moduli of aluminum is straightforward. First, calculate the charge density and determine the directionality of the bonds in crystalline aluminum and repeat the process for the alloy. Next, determine if there are changes in bond directionality and if these are consistent with an increase in moduli. To this end, the FLASTO [2,3] density functional band-structure techniques have been employed to calculate the energies and charge densities of 32 atom fcc supercells. These supercells were constructed from eight conventional fcc cells, producing a supercell lattice constant twice that of the conventional cubic unit cell. The central atom of this cell can be either aluminum or a lithium atom and in the case of a lithium atom, the next nearest lithium atom is in the fourth coordination sphere. Initially the energies of all aluminum supercells as a function of the aluminum-aluminum distance were calculated. The minimum energy obtained corresponded to a near neighbor distance of 0.280 27 nm. This is about 2% smaller than the experimentally determined distance of 0.286 29 nm. All calculations of the aluminum moduli used this aluminum-aluminum separation. For the aluminum-lithium alloy, the central aluminum atom is substituted with a lithium atom producing a supercell of the composition $Al_{31}Li_1$ (modeling an alloy of slightly more than 3 at. % Li). The experimentally determined average first neighbor atomic distance for this composition is 0.286 22 nm. However, the appropriate aluminum-aluminum and aluminum-lithium distances contributing to this average are unknown. Starting with equal aluminum-lithium and aluminum-aluminum first neighbor spacing of 0.286 22 nm, the aluminum-lithium distance was allowed to expand while the aluminum-aluminum distance contracted at a rate which kept the average atomic volume constant. The energy for each aluminum-lithium separation was determined and the minimum obtained at a separation of 0.287 15 nm, making the aluminum-aluminum separation 0.285 29 nm. This ratio was maintained when calculating the shear moduli of the aluminum-lithium alloy.

As shear distortions in a cubic material are symmetric, the energy of only one distortion, along with the equilibrium lattice energy, is the minimum information required to provide an estimate of one of the shear moduli in an fcc metal. In this case, the C_{44} lattice constant was computed by compressing one face diagonal of the supercell by 2% while expanding the perpendicular diagonal of the same face by an amount ($\approx$2%) that keeps the cell volume constant. For the C' elastic constant, the modeled distortion shortens the x coordinate of atoms by 2% while lengthening the y coordinate, again by an amount which holds the cell volume constant ($\approx$2%). The curvature of the energy versus distortion curves gives the elastic moduli and is easily determined by fitting a parabola through these points.

Table I shows the experimentally and computationally determined values of the shear moduli of aluminum and aluminum with $\approx$3 at. % lithium. Though the calculated shear moduli are about 17% stiffer than the true values, there is a uniform increase in both shear elastic constants due to lithium. These increases are of the same relative magnitude as measured experimentally. Table II reports the values of the principal curvatures and the value of the charge density at the aluminum-aluminum bond critical point. From these parameters, the bond directionalities ($\tan\theta$ and $\tan\phi$) can be determined and are reported in the last two columns of Table II.

The effect of lithium substitutions is to increase the directionality of aluminum-aluminum bonds, i.e., to increase the values of $\tan\theta$ and $\tan\phi$. Through the correlation presented in Ref. [1] and depicted in Fig. 3, such an increase will act to stiffen the shear moduli of an fcc metal. Thus, the changes in the character of the charge density at the bond cps are consistent with both the computationally and experimentally determined changes in elastic properties of

TABLE I. In megabar, a comparison of measured and calculated values of the elastic constants of aluminum and $Al_{31}Li$.

	Measured $2C'$	Calculated $2C'$	Measured C_{44}	Calculated C_{44}
Al	0.5238	0.6128	0.3162	0.3592
$Al_{31}Li$	~0.5521	0.6428	~0.3352	0.3776

TABLE II. Principal curvatures at the Al-Al bond critical point of crystalline aluminum and the aluminum-lithium alloy. The density is in terms of electrons per cubic bohr. The curvatures in Heckers, Hk (electrons per bohr^5).

	ρ_0	$\rho_{\parallel\parallel}$	$\rho_{\perp\perp}$	$\rho_{\perp'\perp'}$	$\tan\theta$	$\tan\phi$
Al	0.0321	0.0127	−0.0021	−0.0072	0.407	0.753
$Al_{31}Li$	0.0329	0.0130	−0.0026	−0.0083	0.447	0.799

aluminum-lithium alloys. However, one can reasonably ask if it was necessary to perform such large calculations in order to predict the changes to θ and ϕ.

In the dilute regime, the principal electronic effect produced by a lithium atom substituting for an aluminum atom is to empty states near the Fermi energy, effectively shifting the alloy Fermi energy down relative to the rigid aluminum band. There will then be secondary effects of screening and relaxation that must be considered in order to compute the total energy of the resulting lattice. However, the change in the charge density can be ascertained from knowledge of the Fermi energy charge density alone. In the case of Al, the band diagram can be readily unfolded to show that the major contributions to the Fermi energy charge density are from p-π orbitals. When lithium, in dilute quantities, is substituted for aluminum, these orbitals empty and cease to contribute to the total charge density. By definition a π orbital has zero electron density along the internuclear axis (the bond path). Consequently, removal of electrons from this orbital will have no first order effect on the value of ρ_0 or $\rho_{\parallel\parallel}$. However, a π-bonding orbital must show an increase in charge density as one moves perpendicular to the internuclear axis and must therefore contribute *positive* curvature to $\rho_{\perp\perp}$ and $\rho_{\perp'\perp'}$. Removing electrons from such an orbital will make the negative eigenvalues at a bond critical point more negative, and with no change in $\rho_{\parallel\parallel}$ this must increase $\tan\theta$ and $\tan\phi$. In an fcc metal removing charge from π-bonding orbitals will act to stiffen the metal's elastic shear constants.

Though for heuristic purposes it may prove advantageous to rationalize changes in charge density geometry in terms of the bonding character (δ, π, σ bonding and antibonding) of the orbitals being occupied or emptied, this clearly is not intrinsic to the model presented here. The only parameter that is of significance is the shape of the Fermi energy charge density around a bond critical point. With this knowledge alone, the effects of dilute substitutional impurities on elastic moduli in alloys with an fcc derived structure can be predicted. In alloys with more complex crystallography, the approach may still be applicable, though in some modified form that accounts for all the different bonds that may be present.

Support from the Air Force Office of Scientific Research, the Defense Advanced Research Projects Administration, and the donors to the Petroleum Research Fund of the American Chemical Society are gratefully acknowledged. The author also thanks Dr. Ledbetter for sharing his valuable insight.

[1] M. E. Eberhart, Acta Mater. **44**, 2495 (1996).
[2] J. W. Davenport, Phys. Rev. B **29**, 2896 (1984).
[3] G. W. Fernando, J. W. Davenport, R. E. Watson, and M. Weinert, Phys. Rev. B **40**, 2757 (1989).
[4] Z. Reullaux, Metallika **16**, 436 (1924).
[5] C. Zener, Acta Crystallogr. **2**, 163 (1949).
[6] B. Noble, S. Harris, and K. Dinsdale, J. Mater. Sci. **17**, 461 (1982).
[7] W. Müller, E. Bubeck, and V. Gerold, in *Aluminum Lithium Alloys III* (Institute of Metals, London, 1986), p. 435.
[8] W. Müller, Ph.D. thesis, University of Stuttgart, 1985.
[9] C. N. Lee and J. Kozol, JOM **42**, 11 (1990).
[10] W. Lacom, Mater. Sci. Forum **13/14**, 69 (1987).
[11] E. A. Starke, Jr. and J. T. Staley, Prog. Aerosp. Sci. **32**, 131 (1996).
[12] K. Fuchs, Proc. R. Soc. London A **153**, 622 (1936); **157**, 444 (1936).
[13] J. Thomas, Ph.D. thesis, University of Illinois, Urbana-Champaign, 1968.
[14] J. Thomas, Phys. Rev. **175**, 955 (1968).
[15] T. Suzuki, Phys. Rev. B **3**, 4007 (1971).
[16] H. Ledbetter and T. Suzuki (unpublished).
[17] S. Benckert, Phys. Status Solidi (a) **69**, 483 (1975).
[18] C. Woodward, D. Dimiduk, and S. Rao, J. Met. **50**, 37 (1998).
[19] D. Iotova, N. Kioussis, and S. P. Lim, Phys. Rev. B **54**, 14 413 (1996).
[20] C. Woodward, S. Kajihara, and L. H. Yang, Phys. Rev. B **57**, 13 459 (1998).
[21] C. Woodward, M. Afta, G. Kresse, and J. Hafner, Phys. Rev. B **63**, 094103 (2001).
[22] R. F. W. Bader and H. J. T. Preston, Int. J. Quantum Chem. **3**, 327 (1969).
[23] R. F. W. Bader, P. M. Beddall, and J. Peslak, Jr., J. Chem. Phys. **28**, 557 (1973).
[24] G. R. Runtz, R. F. W. Bader, and R. R. Messer, Can. J. Chem. **55**, 3040 (1977).
[25] R. F. W. Bader, T. T. Nguyen-Dang, and Y. Tal, Rep. Prog. Phys. **44**, 893 (1981).
[26] R. F. W. Bader and P. J. MacDougall, J. Am. Chem. Soc. **107**, 6788 (1985).
[27] P. F. Zou and R. F. W. Bader, Acta Crystallogr. Sect. A **50**, 714 (1994).